



Research Paper

Molecular basis and restoration of function deficiencies of Kv7.4 variants associated with inherited hearing loss

Xin Xia ^a, Qiansen Zhang ^{b, **}, Yanyan Jia ^a, Yilai Shu ^c, Juanmei Yang ^c, Huaiyu Yang ^b, Zhiqiang Yan ^{a, *}

^a State Key Laboratory of Medical Neurobiology and MOE Frontiers Center for Brain Science, Human Phenome Institute, Ministry of Education Key Laboratory of Contemporary Anthropology, Collaborative Innovation Center of Genetics and Development, Institute of Brain Science, Department of Physiology and Biophysics, School of Life Sciences, Fudan University, 2005 Songhu Road, Yangpu District, Shanghai, 200438, China

^b Shanghai Key Laboratory of Regulatory Biology, Institute of Biomedical Sciences, School of Life Sciences, East China Normal University, 500 Dongchuan Road, Minhang District, Shanghai, 200241, China

^c Department of Otolaryngology, Eye & ENT Hospital of Fudan University, Research Institute of Otolaryngology, Fudan University, 83 Fenyang Road, Xuhui District, Shanghai, 200031, China

ARTICLE INFO

Article history:

Received 22 September 2019

Received in revised form

12 December 2019

Accepted 31 December 2019

Available online 3 January 2020

Keywords:

DFNA2

Kv7.4

Hearing loss

Patch-clamp recording

Molecular dynamics simulation

ABSTRACT

Deafness non-syndromic autosomal dominant 2 (DFNA2) is characterized by symmetric, predominantly high-frequency sensorineural hearing loss that is progressive across all frequencies. The disease is associated with variants of a potassium voltage-gated channel subfamily Q member 4 gene, *KCNQ4* (Kv7.4). Here, we studied nine recently identified Kv7.4 variants in DFNA2 pedigrees, including V230E, E260K, D262V, Y270H, W275R, G287R, P291L, P291S and S680F. We proved that the variant S680F did not alter the channel function while the other eight variants resulted in function deficiencies. We further proved that the two variants E260K and P291S showed reduced cell membrane expressions while the other seven variants showed moderate cell surface expressions. Thus, trafficking deficiency is not a common mechanism underlying channel dysfunction. Next, we studied two variants, V230E and G287R, using molecular dynamics simulation. We showed that V230E stabilized Kv7.4 channel in the closed state by forming an additional hydrogen bond with a basic residue K325, while G287R distorted the selectivity filter and blocked the pore region of Kv7.4 channel. Moreover, by co-expressing wild-type (WT) and variant proteins *in vitro*, we demonstrated that the heterogeneous Kv7.4 channel currents were reduced compared to the WT channel currents and the reduction could be rescued by a Kv7.4 opener retigabine. Our study provided the underlying mechanisms and suggested a potential alternative therapeutic approach for DFNA2.

© 2020 Elsevier B.V. All rights reserved.

1. Introduction

Hearing loss is one of the most common genetic sensory defects in human beings. Approximately 80% of inherited deafness instances are a non-syndromic hearing loss (NSHL) (Posukh et al., 2005). The genetic forms of NSHL contain X-linked (DFN), autosomal dominant (DFNA) and autosomal recessive (DFNB) modes, as well as mitochondrial forms which results from changes to mtDNA. DFNA2 is named as the second loci to be found in DFNA subtype,

characterized by progressive and predominantly high-frequency sensorineural hearing loss. DFNA2 is genetically related to Kv7.4 variants (Goldstein and Lalwani, 2002; Kubisch et al., 1999). Until now, 30 Kv7.4 variants have been identified in pedigrees of autosomal dominant hearing loss (Table S1) (Abdelfatah et al., 2013; Akita et al., 2001; Arnett et al., 2011; Baek et al., 2011; Coucke et al., 1999; de Heer et al., 2011; Hildebrand et al., 2008; Huang et al., 2017; Ishikawa et al., 2014; Jung et al., 2018; Kamada et al., 2006; Mencia et al., 2008; Naito et al., 2013; Namba et al., 2012; Shin et al., 2018; Su et al., 2007; Talebizadeh et al., 1999; Topsakal et al., 2005; Uehara et al., 2015; Van Camp et al., 2002; Van Hauwe et al., 2000; Wang et al., 2014; Wasano et al., 2015; Watabe et al., 2013; Wu et al., 2013).

Kv7.4 channel belongs to a family of voltage-gated potassium

* Corresponding author.

** Corresponding author.

E-mail addresses: qs Zhang@bio.ecnu.edu.cn (Q. Zhang), zqyan@fudan.edu.cn (Z. Yan).

channels, Kv7 channels. Kv7 channels are composed of four subunits and generate outward currents under voltage stimulation. Kv7 channels, also known as M channels, are suppressed by stimulating muscarinic acetylcholine receptors (Wang and Li, 2016). M channels repolarize cells, reduce cell excitability and regulate many physiological responses (Kubisch et al., 1999). Kv7.4 is mainly expressed in the cochlea, vestibule, central auditory pathway, heart and smooth muscle tissues (Barrese et al., 2018; Bientinesi et al., 2017; Chadha et al., 2014; Hansen et al., 2008; Iannotti et al., 2013; Jepps et al., 2009, 2011; Kharkovets et al., 2000; Kubisch et al., 1999; Testai et al., 2016; Wei et al., 2018). In the cochlea, Kv7.4 is specifically expressed in the sensory outer hair cells (OHCs) (Kubisch et al., 1999). Moreover, the expression of Kv7.4 in the apical OHCs is weaker than that of the basal ones (Kharkovets et al., 2000). This phenomenon is intriguing since basal OHCs are known to be responsible for high frequency hearing (Kharkovets et al., 2000). Correspondingly, in the mouse model, the variant of Kv7.4 (G286S) results in degeneration of OHCs, which is known as the mechanism underlying DFNA2 (Kharkovets et al., 2006).

It has been reported that several Kv7.4 variants (L274H, W276S, L281S, G285C, and G296S) induced channel function loss that underlies the cellular mechanisms of DFNA2 (Kim et al., 2011). However, a growing number of new Kv7.4 variants have been identified in DFNA2 pedigrees (Arnett et al., 2011; Hildebrand et al., 2008; Naito et al., 2013; Namba et al., 2012; Wang et al., 2014; Wu et al., 2013). Linkage analysis and genotyping have been used to reveal the role of the Kv7.4 variants in the molecular etiology of inherited deafness (Arnett et al., 2011; Hildebrand et al., 2008; Naito et al., 2013; Namba et al., 2012; Wang et al., 2014; Wu et al., 2013). Nevertheless, a functional study is still needed to demonstrate the correlations between the Kv7.4 variants and hearing loss. Here, we investigated the underlying molecular mechanisms of nine recently identified DFNA2 related Kv7.4 variants (V230E, E260K, D262V, Y270H, W275R, G287R, P291L, P291S and S680F).

2. Materials and methods

2.1. Plasmid construct

The WT Kv7.4 (isoform a, gene ID: NM_004700.4, OMIM reference number: 603537) plasmid (EX-U0210-M98-5) containing a fusion GFP was purchased from GeneCopoeia and used for electrophysiological recording. The fusion GFP in the plasmid EX-U0210-M98-5 was substituted with mCherry by homologous recombination method and verified by automated sequencing for the co-transfection experiments. Kv7.4 variants used in the electrophysiological recordings were generated from the WT Kv7.4 gene in the plasmid EX-U0210-M98-5 by homologous recombination method and verified by automated sequencing. For detection of cell surface expressions of the WT and variant Kv7.4 channels, c-Myc epitope was inserted into the plasmid EX-U0210-M98-5. The modified c-Myc tag was inserted into the Kv7.4 channel as described previously (Kim et al., 2011). The WT Kv7.4 gene was subcloned to a pIRES2-EGFP plasmid using homologous recombination method for the related experiment.

2.2. Cell culture and transfection

Chinese hamster ovary (CHO) cell line was cultured in F-12/DMEM media with 10% fetal bovine serum (FBS) and 1% antibiotic-antimycotic mixture (Invitrogen) at 37 °C with 5% CO₂. Plasmid was transiently transfected into cells, at a total amount of 3000 ng per dish in 35 mm culture dishes, using Lipofectamine 3000 (Invitrogen) according to the manufacturer's instructions.

2.3. Electrophysiological recording

Whole-cell voltage-clamp recordings were performed using an Axopatch 700B amplifier (Axon Instruments, USA) at room temperature (20–24 °C). For patch pipette preparation, the borosilicate glass pipettes (BF150-86-10, Sutter Instrument, Novato) were pulled using a Flaming/Brown micropipette puller (P-97, Sutter Instrument, Novato) and polished to a diameter corresponding to a pipette resistance in the range of 3–6 MΩ. The pipette solution contained (in mM): 140 KCl, 1 MgCl₂, 10 HEPES, 10 EGTA, 1 CaCl₂, 4 K₂ATP, pH 7.2 adjusted with KOH. The bathing solution contained (in mM): 145 NaCl, 4 KCl, 1.8 CaCl₂, 0.5 MgCl₂, 10 HEPES, 5 D-glucose, pH 7.3 adjusted with NaOH. Retigabine (S4733, Selleck, USA) was applied in the bath solution at 10 μM concentration. Signals were filtered at 1 kHz and digitized using a DigiData 1550 with pClamp 10.5 software (Molecular Devices, USA). The pipette off-set was corrected after the pipette entered the bath solution. C-fast cancellations were done once a GΩ seal has been formed. Whole-cell capacitance compensation was performed after the cell membrane was broken. P/N leak subtraction was performed and the serial resistance was monitored throughout the experiments. We discarded the poor quality recordings which have a serial resistance over 15 MΩ. The Kv7.4 channel current traces were generated by voltage steps ranging from –100 to 40 mV with 20 mV increments from a holding potential of –80 mV. The currents at different voltage potentials were measured at peak levels. The currents were then divided by the cell capacitance (pF) to generate the current density-voltage relationship. Analyses of data were performed with GraphPad Prism7. Pooled data are shown as means ± SEM. Data were analyzed with logarithmic transformation by unpaired *t*-test.

2.4. Immunostaining and confocal imaging

The primary antibody used was mouse monoclonal anti-c-Myc (abs830004, absin) in 1 μg/ml concentration. The secondary antibody was Alexa Fluor 594 AffiniPure Donkey Anti-Mouse IgG (34112ES60, YEASEN) in the manufacturer's recommended concentration. After transfection for 24 h, cells were fixed in 4% paraformaldehyde in 1 × phosphate-buffered saline (PBS) for 10 min. PBS washing was needed before the next step. To perform intracellular staining (i.e. the P state), cells were permeabilized and blocked at 37 °C in 0.1% Triton X-100 and 3% bovine serum albumin (BSA) in PBS for 30 min. To operate plasma membrane staining (i.e. the NP state), cells were blocked in 3% BSA in 1 × PBS at 37 °C. After blocking, incubation in primary antibody at 4 °C overnight followed, three times of PBS washing was needed before the next move. After that, cells were incubated in secondary antibody at room temperature for 90 min. At last, DAPI staining for 5 min was conducted. Fluorescent images were taken on a confocal microscope (FV1200, OLYMPUS, Japan) with Fluoview software. Images were acquired using a 60 × oil immersion objective with a pixel format of 1600 × 1600.

2.5. Surface Kv7.4 protein isolation and western blot

CHO cells in 10 cm culture dishes were transfected with c-Myc tagged WT or mutant Kv7.4 respectively (12 μg per dish). 24 h after transfection, cells were washed twice with PBS for 5 min each and incubated with monoclonal anti-c-Myc antibody (abs830004, absin) in 1 μg/ml concentration for 30 min at room temperature. After incubation, cells were washed three times for 5 min each. After washes, cells were collected in fresh tubes and lysed with 900 μl RIPA lysis buffer (CW2334S, cwbio) supplemented with protease inhibitor cocktail (CW2200S, cwbio), rotating at 4 °C for

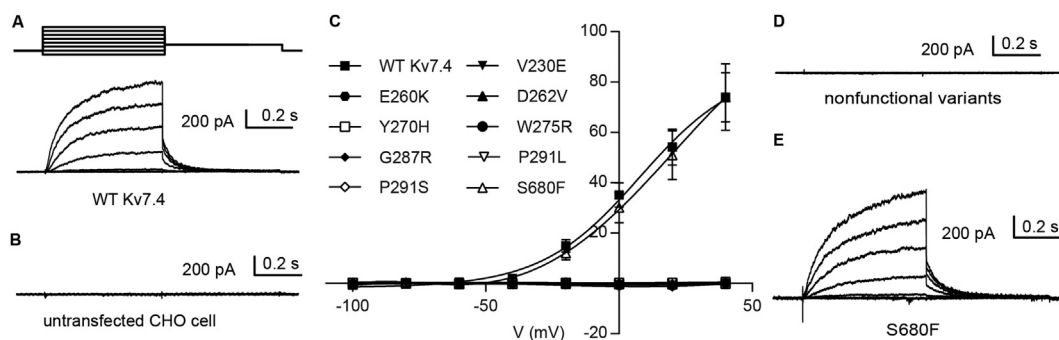


Fig. 1. Whole-cell currents of wild-type (WT) and variant Kv7.4 channels expressed in CHO cells. (A) Representative current traces of WT Kv7.4 expressed in CHO cells. Cells were held at -80 mV. Step voltages ranged from -100 to 40 mV with 20 mV increments, followed by a pulse of -50 mV. (B) Un-transfected CHO cells yielded no measurable current. The current traces were recorded using the same protocol described in (A). (C) The consistent current density-voltage relationships of WT and variant Kv7.4 channels. WT, $n = 30$. V230E, $n = 6$. E260K, $n = 9$. D262V, $n = 4$. Y270H, $n = 10$. W275R, $n = 8$. G287R, $n = 7$. P291L, $n = 9$. P291S, $n = 10$. S680F, $n = 18$. All error bars denote \pm SEM. (D) Sample traces of nonfunctional variant Kv7.4 channels (V230E, E260K, D262V, Y270H, W275R, G287R, P291L and P291S) recorded utilizing the same protocol depicted in (A). The above variants did not produce detectable current. (E) Sample traces of variant Kv7.4 channel S680F. The variant S680F generated robust currents comparable to that of the WT channels.

30 min. The cell lysate was centrifuged at $14,000$ g for 10 min at 4 °C. 100 μ l of each supernatant was kept in another tube as an input sample. Input samples were heated at 95 °C for 10 min with 25 μ l of $5 \times$ sodium dodecyl sulfate polyacrylamide gel electrophoresis (SDS-PAGE) Loading Buffer (CW0027S, cwbio). The rest of the supernatant was incubated with 50 μ l Dynabeads Protein G (10003D, Invitrogen) at room temperature for 30 min. After incubation, beads were washed three times with 200 μ l 0.02% Tween-20 in cold PBS. After washing, proteins were eluted from beads with 50 μ l of $1 \times$ SDS-PAGE Loading Buffer at 70 °C for 5 min. Proteins were separated on 12% SDS-PAGE gels and transferred to nitrocellulose membranes (1620115, Bio-Rad) using standard procedures. c-Myc-tagged Kv7.4 proteins were detected with monoclonal anti-c-Myc antibody (abs830004, absin) and HRP-labeled Goat Anti-Mouse IgG(H + L) (A0216, beyotime). Actin proteins were detected with Anti-ACTB mouse monoclonal antibody (D190606, Sangon Biotech) and HRP-labeled Goat Anti-Mouse IgG(H + L). The bands on the membranes were visualized by Immun-Star HRP Substrate (1705041, Bio-Rad). Chemiluminescent signals were collected by ChemiDoc Imaging System and Image Lab software (Bio-Rad, USA).

2.6. Simulation systems built

As there is no Kv7.4 crystal structure, the open and closed state Kv7.4 channel structural models were generated by homology modeling using Kv7.4 sequence (P56696) from Uniprot (Bateman et al., 2015). The crystal structures of Kv1.2 (PDB code: 2A79) (Long et al., 2005) and Kv7.1 (PDB code: 5VMS) (Sun and MacKinnon, 2017) provide the information about Kv open and closed state conformation. Based on these structural information, we modeled the Kv7.4 transmembrane domains in open- and closed-states. Multiple sequence alignments of the templates and Kv7.4 were performed by using the ClustalW Web server (<http://www.clustal.org/>), and the highly conserved residues were used to guide the alignment. After manually adjusting the alignments, homology models of the Kv7.4 channel in the open and closed states were built with program MODELLERv9.19 (Eswar et al., 2008). The structure models for V230E and G287R Kv7.4 variants used for molecular dynamics (MD) simulation were built from the closed and open state Kv7.4 model by mutating V230E or G287R.

The V230E and G287R variant Kv7.4 models were embedded separately into a POPC bilayer by aligning the protein's axis of symmetry with the bilayer normal. In each system, lipids located within 1 Å of the Kv7.4 channel were removed. Subsequently, each

system was solvated by TIP3P waters with 0.15 M KCl. Each simulation system included $\sim 200,000$ atoms (140 Å \times 140 Å \times 110 Å).

2.7. MD simulation

All MD simulations were performed using the GROMACS 5.1 package (Abraham et al., 2015) with the Isobaric-Isothermal (NPT) ensemble and the CHARMM36-CMAP force field (Klauda et al., 2010). Energy minimizations were first performed to relieve unfavorably contacts, followed by equilibration steps of 22 -ns in total to equilibrate the lipid bilayer and the solvent, with restraints (isotropic force constant $\kappa = 1 \times 10^3$ kJ mol $^{-1}$ nm $^{-2}$) on the main chain of the receptors. Subsequently, a 500 -ns all-atom MD simulation was performed for each system. The temperature of each system was maintained at 300 K using the v-rescale method (Bussi et al., 2007) with a coupling time of 0.1 ps. The pressure was kept at 1 bar using the Berendsen barostat (Berendsen et al., 1984) with $\tau_p = 1.0$ ps and compressibility of 4.5×10^{-5} bar $^{-1}$. SETTLE (Bussi et al., 2007) constraints and LINCS (Hess et al., 1997) constraints were applied to the hydrogen-involving covalent bonds in water molecules and other molecules, respectively, and the time step was set to 2 fs. Electrostatic interactions were calculated with the Particle-Mesh Ewald (PME) algorithm (Kholmurov et al., 2000) with a real-space cutoff of 1.4 nm. Analysis of the trajectories was performed using Gromacs analysis tools. PyMOL (The PyMOL Molecular Graphics System, Version 1.3, Schrödinger, LLC) was used to visualize the structure models and generate figures.

3. Results

3.1. Kv7.4 variants induced channel function deficiency

To examine the functional properties of Kv7.4 variants, the WT and nine variant Kv7.4 channels (V230E, E260K, D262V, Y270H, W275R, G287R, P291L, P291S and S680F) were heterologously expressed in CHO cells, respectively. We used the fusion GFP in the vector as the transfection marker. Under the voltage steps ranging from -100 mV to 40 mV from a holding potential of -80 mV, cells transfected with WT Kv7.4 produced robust outward currents (Fig. 1A). In addition, no measurable current was detected in untransfected CHO cells under the same stimulation (Fig. 1B), which further validated the channel activity of Kv7.4. We also proved that the fusion GFP in the vector didn't affect the Kv7.4 channel activity (Fig. S2). The current density of WT Kv7.4 channels at 40 mV was 74.0 ± 9.8 pA/pF ($n = 30$) (Fig. 1C).

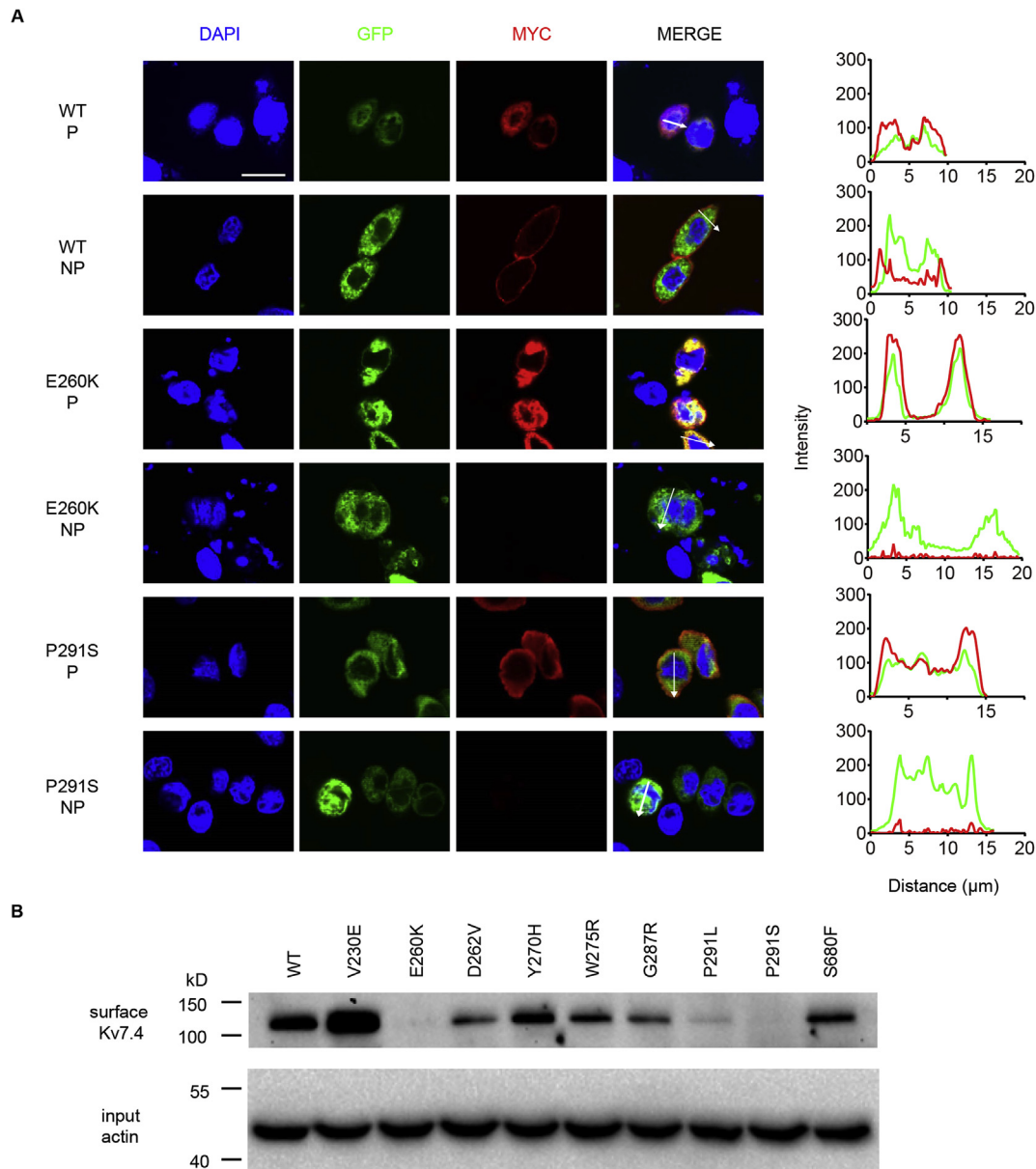


Fig. 2. Detection of cell surface expressions of wild-type (WT) and variant Kv7.4 channels. (A) Representative pictures showing WT and variant Kv7.4 channels' expressions in CHO cells. In non-permeabilized (NP) state, the anti-c-Myc antibody stained only the Kv7.4 protein expressed on the cell surface. In permeabilized (P) state, the anti-c-Myc antibody stained protein expressed on the cell surface and in the cytoplasm. Fluorescent intensities of GFP (green) and Kv7.4 channels (red) were delineated against the distance, which was marked with the white arrow in the merged image. The scale bar is 10 μm. (B) Representative western blot. Surface Kv7.4 proteins were isolated from transfected CHO cells. The Kv7.4 variants E260K and P291S could not be detected in the cell surface. The surface expressions of the WT channels and the other seven variants (V230E, D262V, Y270H, W275R, G287R, P291L and S680F) were detected.

We then examined the channel activities of Kv7.4 variants with the same protocol. Comparing with the WT Kv7.4 channel, no measurable outward current was recorded in the variants V230E, E260K, D262V, Y270H, W275R, G287R, P291L and P291S (Fig. 1C–D). The results showed that the above eight variants induced channel function deficiency. However, the variant S680F generated outward currents that were comparable to the WT channels (Fig. 1C and 1E). The current density of variant S680F at 40 mV was 74.0 ± 13.2 pA/pF ($n = 18$), equal to that of the WT channels (Fig. 1C). The results suggested that the variant S680F did not destroy the channel activity of Kv7.4 channels.

3.2. Cell surface expressions of Kv7.4 variants

A previous study suggested that five Kv7.4 variants (L274H, W276S, L281S, G285C, and G296S) generated non-functional channels because of defective membrane trafficking (Kim et al., 2011). In addition, two variants (F182L and D266Y, located in the transmembrane domain) did not show defect in Kv7.4 trafficking to the plasma membrane (Jung et al., 2018; Kim et al., 2011). From these studies (Jung et al., 2018; Kim et al., 2011), it seems that the variants with transmembrane domain residues mutating into polarity residues may affect Kv7.4 trafficking to the membrane. However, the variants with transmembrane domain residues mutating into hydrophobic residues may not damage membrane

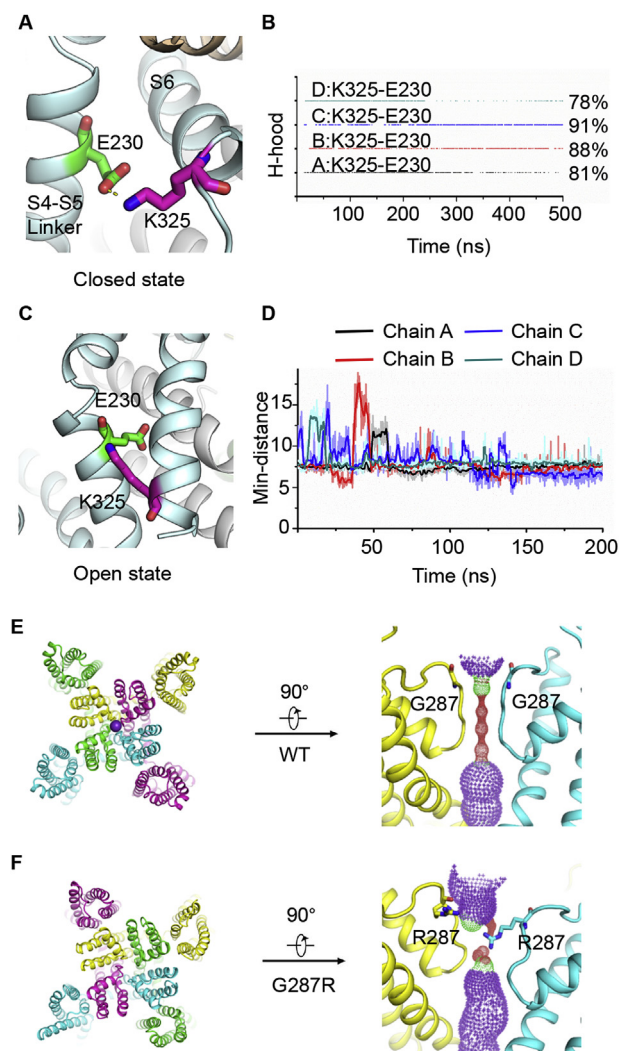


Fig. 3. Simulation of Kv7.4 variants V230E and G287R. (A) Closed state view of the structural model of Kv7.4 variant V230E. E230 and K325 were labeled. (B) Evaluation of the hydrogen bond between E230 and K325 over 500-ns simulation. (C) Open state view of the structural model of Kv7.4 variant V230E. (D) Minimal distances of E230 and K325 side chains in open state Kv7.4 variant V230E during the 200-ns molecular dynamics simulation. (E) The structural model of wild-type (WT) Kv7.4. The selectivity filter was labeled and the solvent-accessible (mesh) pore lined with residue G287. The purple ball represented potassium ion. (F) The structural model of Kv7.4 variant G287R. The G287 and the R287 residues were shown as sticks.

trafficking. We also speculated that variants which are not located in the transmembrane domain may not affect membrane trafficking. Based on this inference, we predicted whether the above nine Kv7.4 variants would result in abolished membrane trafficking. We predicted that variants V230E, E260K, G287R and P291S would induce defective membrane trafficking, while D262V, Y270H, W275R, P291L and S680F would not affect the trafficking process.

To verify our predicted results, we examined the cell surface expressions of the WT and variant Kv7.4 channels by immunostaining. c-Myc tag was inserted into the extracellular region between S1-S2 transmembrane domains. And we verified that this tag did not affect the Kv7.4 channel activity (Fig. S3). In permeabilized (P) state, the expressions of the variant channels couldn't be distinguished from that of the WT channels (Fig. 2A; Fig. S4). As determined in Fig. 2A, WT Kv7.4 channels were labeled in the

plasma membrane in non-permeabilized (NP) state. We further proved that the two variant channels (E260K and P291S) showed defective expressions in the cell membrane (Fig. 2A), consistent with the five Kv7.4 variants (L274H, W276S, L281S, G285C, and G296S) reported previously (Kim et al., 2011). We detected the variant S680F in the cell surface (Fig. S4). Unexpectedly, we found that the other six variants (V230E, D262V, Y270H, W275R, G287R and P291L) were localized in the plasma membrane (Fig. S4).

To confirm these results, we further conducted western blot to analyze the surface expressions of the WT and variant Kv7.4 channels. The surface Kv7.4 protein was isolated from CHO cells transfected with the WT or variant c-Myc tagged Kv7.4 with a fusion GFP, respectively. As shown in Fig. 2B, the WT Kv7.4 channels were localized in the plasma membrane, while the Kv7.4 variants E260K and P291S could not be detected in the plasma membrane. The surface expressions of the other seven variants (V230E, D262V, Y270H, W275R, G287R, P291L and S680F) were detected (Fig. 2B), consistent with our immunostaining results (Fig. S4). These results revealed that the six variants (V230E, D262V, Y270H, W275R, G287R and P291L) expressed in the plasma membrane despite of channel function loss. The results suggested that trafficking deficiency might not be a common mechanism for channel loss of function in Kv7.4 variants and raised the necessity to explore the underlying mechanisms.

3.3. Structural basis of Kv7.4 variants causing the channel dysfunction

Although most of the experimental results were consistent with the predicted results, two variants, V230E localized in the S4-S5 linker and G287R localized in the pore domain, were found to be correctly targeted to the cell surface, however lacked voltage dependent currents. To decipher how V230E and G287R variants disable the Kv7.4 channel function, we performed all-atom molecular dynamics (MD) simulation to determine the structural mechanisms of variant induced channel loss of function. Using homology modeling and the crystal structures of Kv7.1 (Sun and MacKinnon, 2017) and Kv1.2 (Long et al., 2005), we built the models of the Kv7.4 channel in its closed and open states, respectively. V230E and G287R Kv7.4 models were built from the closed state Kv7.4 model by mutating V230E or G287R. The V230E and G287R models were embedded into a palmitoylcholine (POPC) bilayer, and two simulation systems were built. Subsequently, 500-ns MD simulation was performed with each simulation system.

Fig. 3A showed the last snapshot conformation from the MD simulation of closed state V230E model. From that, we observed that E230 directly interacted with a positively charged residue K325 at the C-terminus of the S6 segment in the same subunit of the closed state Kv7.4 channel. The MD simulation indicated that once the salt bridges emerged between E230 and K325, the interaction was very stable. The salt bridges were present >78% of the time during the 500-ns MD simulation in the four subunits (Fig. 3B). We then performed another 200-ns MD simulation based on the V230E open state Kv7.4 channel model to investigate the contribution of the salt bridges E230-K325 to channel gating. In contrast, during the open state V230E variant model MD simulation, E230 was not able to form the same interaction with K325, as the E230 swung to the opposite direction, comparing to E230 in the closed state (Fig. 3C). The minimal distance between the side chains of K325 and E230 is basically maintained at about 7 Å during the MD simulation (Fig. 3D). And within these distances, E230 cannot form a stable salt bridge with K325. Thus, these additional salt bridges E230-K325 in the Kv7.4 closed conformation acted like a lock, fixing the Kv7.4 channel in closed state. On the other hand, it

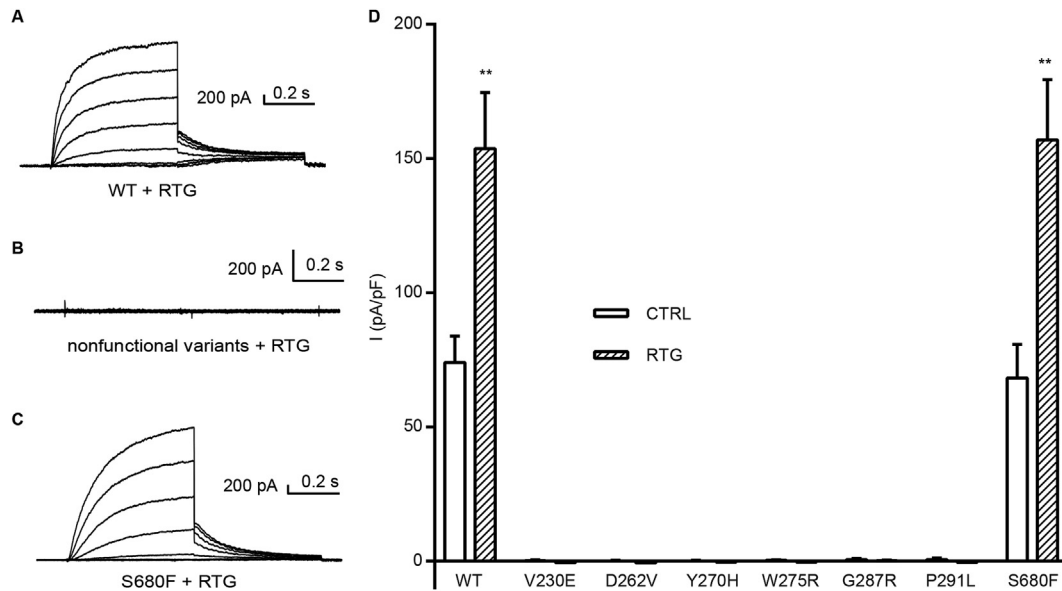


Fig. 4. Whole-cell currents of wild-type (WT) and variant Kv7.4 channels in the presence of retigabine (RTG). (A–C) Representative current traces of WT and variant Kv7.4 channels [WT (A), nonfunctional variants (V230E, D262V, Y270H, W275R, G287R, P291L) (B) and S680F (C)] in the presence of 10 μ M RTG. Currents were recorded utilizing the same protocol depicted in the legend of Fig. 1A. (D) The mean current densities of WT and variant Kv7.4 channels at 40 mV in the absence or presence of 10 μ M RTG. WT, n = 30. V230E, n = 6. D262V, n = 4. Y270H, n = 10. W275R, n = 8. G287R, n = 7. P291L, n = 9. S680F, n = 18. WT + RTG, n = 30. V230E + RTG, n = 4. D262V + RTG, n = 4. Y270H + RTG, n = 4. W275R + RTG, n = 4. G287R + RTG, n = 4. P291L + RTG, n = 4. S680F + RTG, n = 7. All error bars denote \pm SEM. **, $p < 0.01$.

did not contribute to the stabilization of the Kv7.4 channel open conformation. Conclusively, the variant V230E in Kv7.4 urged the channel tend to maintain closed state and prevented the Kv7.4 channel opening.

G287 is a highly conserved pore residue in the Kv7 channels (Fig. S1B). As this residue locates in the selectivity filter domain of Kv7.4 channel, we tested whether G287R variant altered the selectivity filter architecture of Kv7.4 channel. In the WT Kv7.4 channel, the selectivity filter distributed equally (Fig. 3E), which defined the potassium ion permeant substrate profile. The simulation of Kv7.4 variant G287R indicated that R287 blocked the selectivity filter domain. In the G287R simulation, the selectivity filter was distorted and the residue of R287 stretched into this domain and blocked the pore region after 500-ns simulation (Fig. 3F). In conclusion, the variant G287R disrupted the selectivity filter domain and induced channel dysfunction.

3.4. Channel opener potentiated the reduced currents of the heterogeneous Kv7.4 channels mimicking DFNA2 patients genotype

Retigabine (RTG) is an opener of Kv7.2–7.5 (Gunthorpe et al., 2012). The WT Kv7.4 channel currents were significantly potentiated by the application of 10 μ M RTG (Fig. 4A and 4D). We wondered if RTG could activate the variant Kv7.4 channels expressed in the cell membrane. As determined in Fig. 4, in the presence of 10 μ M RTG, the variant Kv7.4 channels (V230E, D262V, Y270H, W275R, G287R and P291L) did not generate measurable outward currents. The current densities of the above variant Kv7.4 channels at 40 mV were indistinguishable in the absence or presence of RTG (Fig. 4D), indicating that RTG had no effect on the above variants. In addition, we observed that RTG could also activate the channel currents of the variant S680F (Fig. 4C and 4D).

In DFNA2 patients, missense variants were presented in a heterozygous state (Coucke et al., 1999; Kubisch et al., 1999). To investigate the pathology of DFNA2 by mimicking the heterozygous genotype of patients, we co-transfected the WT and variant Kv7.4 in CHO cells at ratio 1:1. Comparing with the WT Kv7.4 channels, the

heterogeneous Kv7.4 channels generated reduced currents except for S680F/WT (Fig. 5; Fig. S5). At 40 mV, the WT channels generated robust outward currents and the current density was 74.0 ± 9.8 pA/pF (n = 30) (Fig. 5B). The current density of S680F/WT channels at 40 mV was 70.4 ± 11.3 pA/pF (n = 12) (Fig. 5B), comparable to that of the WT channels. The results showed that the variant S680F did not damage the channel activity of the heterogeneous Kv7.4 channels. The results suggested that the variant S680F might be polymorphism and did not induce DFNA2. Under the same condition, the other eight heterogeneous Kv7.4 channels showed reduced current densities as 27.2 ± 6.6 pA/pF (n = 12) (V230E/WT), 19.9 ± 5.1 pA/pF (n = 12) (E260K/WT), 30.4 ± 6.7 pA/pF (n = 11) (D262V/WT), 38.2 ± 7.8 pA/pF (n = 14) (Y270H/WT), 18.0 ± 3.2 pA/pF (n = 15) (W275R/WT), 32.9 ± 7.2 pA/pF (n = 13) (G287R/WT), 32.9 ± 7.6 pA/pF (n = 11) (P291L/WT), and 39.7 ± 10.8 pA/pF (n = 16) (P291S/WT) (Fig. 5B). The varied current densities suggested that the eight variants disabled channel function of the heterogeneous Kv7.4 channels to varying degrees. We also proved that the half amount of WT Kv7.4 DNA and the fusion mCherry tag used in the co-expression experiments had equal effects on the currents of Kv7.4 channels (Fig. S6).

We then assessed if RTG could restore the channel activities of heterogeneous Kv7.4 channels. As shown in Fig. 5 and Fig. S5, in the presence of 10 μ M RTG, the crippled WT: variant (1:1) currents were strongly potentiated and the reduced current densities of the heterogeneous channels at 40 mV were restored to 63.8 ± 10.6 pA/pF (n = 16) (V230E/WT), 46.6 ± 8.6 pA/pF (n = 13) (E260K/WT), 76.6 ± 16.2 pA/pF (n = 12) (D262V/WT), 71.7 ± 16.8 pA/pF (n = 16) (Y270H/WT), 39.2 ± 10.5 pA/pF (n = 13) (W275R/WT), 58.4 ± 9.8 pA/pF (n = 15) (G287R/WT), 93.3 ± 18.8 pA/pF (n = 14) (P291L/WT) and 72.4 ± 16.3 pA/pF (P291S/WT) (n = 15) (Fig. 5B). So, we concluded that RTG could partially restore the function of the heterogeneous Kv7.4 channels mimicking DFNA2 patients genotype. This result indicated the possibility of an alternative therapeutic approach for DFNA2.

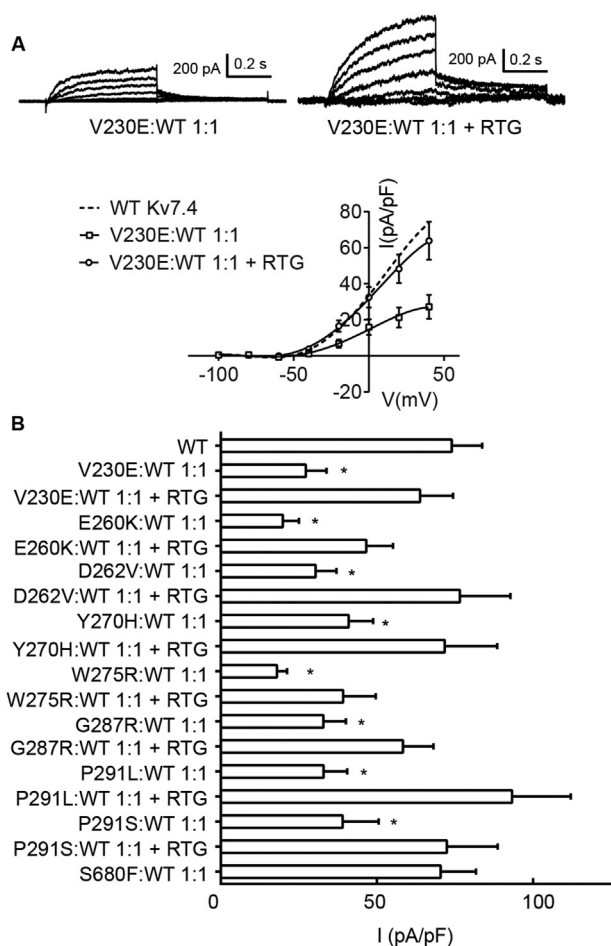


Fig. 5. Electrophysiological properties of heterogeneous Kv7.4 channel currents in the absence or presence of retigabine (RTG). (A) Above, representative traces of currents of CHO cells co-expressing wild-type (WT) and variant Kv7.4 (V230E) at a ratio of 1:1 (the ratio of DNA for transfection) in the absence or presence of RTG, currents were recorded utilizing the same protocol depicted in the legend of Fig. 1A. Below, current density-voltage relationships of the heterogeneous Kv7.4 channels (V230E/WT) in the absence or presence of RTG. All error bars denote \pm SEM. (B) The mean current densities of the WT and heterogeneous Kv7.4 channels at 40 mV in the absence or presence of RTG. All error bars denote \pm SEM. *, $p < 0.05$.

4. Discussion

Variants in the potassium channel gene Kv7.4 have been proved to be associated with DFNA2, a subtype of autosomal dominant, progressive, high-frequency hearing loss. Until now, 30 Kv7.4 variants related to DFNA2 have been identified (Table S1) (Abdelfatah et al., 2013; Akita et al., 2001; Arnett et al., 2011; Baek et al., 2011; Coucke et al., 1999; de Heer et al., 2011; Hildebrand et al., 2008; Huang et al., 2017; Ishikawa et al., 2014; Jung et al., 2018; Kamada et al., 2006; Mencia et al., 2008; Naito et al., 2013; Namba et al., 2012; Shin et al., 2018; Su et al., 2007; Talebizadeh et al., 1999; Topsakal et al., 2005; Uehara et al., 2015; Van Camp et al., 2002; Van Hauwe et al., 2000; Wang et al., 2014; Wasano et al., 2015; Watabe et al., 2013; Wu et al., 2013).

Although it has been verified that Kv7.4 variants induced channel dysfunction as a result of protein trafficking deficiency in CHO cells (Kim et al., 2011), we demonstrated that six function loss variants, V230E, D262V, Y270H, W275R, G287R and P291L were localized in the cell surface. Therefore, impaired cell surface expression might not be a common mechanism underlying channel dysfunction. Due to the limitation of the approach, all the

experiments presented in this work were performed in CHO cells, but not in hair cells, where the mechanisms of surface expressions of membrane proteins might be different. Furthermore, we elucidated the mechanisms of V230E and G287R induced channel dysfunction by MD simulation. The simulation results indicated that there might be possible solutions for restoration of the deficient function of variant Kv7.4 channels. Taking V230E variant as an example, proper compounds binding to specific sites of the Kv7.4 channel might stabilize the channel open conformation and thus rescue the function of variant Kv7.4 channels.

Researchers proposed that the reduced currents of heterogeneous Kv7.4 channels resulted from the dependence of cell surface expression of the variant on the WT subunits (Kim et al., 2011). Here, we proved that the V230E, D262V, Y270H, W275R, G287R and P291L variants expressed on the cell surface without co-expression of the WT subunits. Thus, in DFNA2 etiology, the impaired cell surface expression and altered conductance of the heterogeneous Kv7.4 channels must involve two independent mechanisms.

RTG, as well as zinc pyrithione (ZnPy), another enhancer of Kv7 channels, rescued the function of heterogeneous Kv7.4 channel from DFNA2 variants (D266Y, W276S, G285S, G321S) (Jung et al., 2018; Leitner et al., 2012). A previous study proved that the restoration relied on the potentiation of solely homomeric WT channel currents in pore domain variants and probably both of homomeric WT channel and heterogeneous channel currents in C-terminal variants (Leitner et al., 2012). Here, we proved that RTG could rescue the heterogeneous Kv7.4 channel function from the eight DFNA2 variants located in different domains of Kv7.4. DFNA2 is an autosomal dominant disease. Most of DFNA2 missense variants were presented in a heterozygous state (Coucke et al., 1999; Kubisch et al., 1999). So we concluded that RTG might restore the heterogeneous Kv7.4 channel function from most of DFNA2 variants in spite of their different locations. In addition, RTG is a FDA approved drug for epilepsy (Rudzinski et al., 2016). Since RTG could restore the function of the heterogeneous Kv7.4 channels which mimicking the genotype of DFNA2 patients, it might be an option as an adjunctive therapy for DFNA2 patients. In addition, it was reported that RTG protected against peripheral salicylate ototoxicity in rats (Sheppard et al., 2015). Until now, no agent has been found to selectively activate Kv7.4 channel (Barrese et al., 2018). Efforts have been made in improving the specificity of Kv7.4 activators (Wang et al., 2019). And more research is still needed to identify Kv7.4 specific opener as an alternative therapeutic approach for hearing loss.

5. Conclusions

In this study, we confirmed that Kv7.4 variants, including V230E, E260K, D262V, Y270H, W275R, G287R, P291L and P291S resulted in channel function deficiency, which facilitated the identification of the genetic etiology of DFNA2. Our results also indicated that the variant S680F might be polymorphism and did not induce DFNA2. Moreover, the cell surface expression analysis indicated that trafficking deficiency is not a common mechanism for Kv7.4 channel loss of function caused by variants. By MD simulation, we revealed the intricate mechanisms of variant induced channel dysfunction. In addition, by co-expression *in vitro*, we confirmed that the currents of the combination of WT and variant channels were reduced compared to that of the WT channels and the reduction could be rescued by RTG. Taken together, our findings facilitated the genetic diagnosis of DFNA2, provided insights for the underlying mechanisms of DFNA2 and suggested a possible future therapeutic approach for DFNA2.

CRediT authorship contribution statement

Xin Xia: Methodology, Formal analysis, Investigation, Writing - original draft, Writing - review & editing, Visualization. **Qiansen Zhang:** Methodology, Formal analysis, Investigation, Writing - original draft, Writing - review & editing, Visualization. **Yanyan Jia:** Writing - review & editing, Visualization. **Yilai Shu:** Writing - review & editing. **Juanmei Yang:** Writing - review & editing. **Huaiyu Yang:** Resources, Writing - review & editing, Supervision, Project administration, Funding acquisition. **Zhiqiang Yan:** Conceptualization, Resources, Writing - review & editing, Supervision, Project administration, Funding acquisition.

Acknowledgements

The research was supported by funds from the National Key R&D Program of China Project (2017YFA0103900, 2016YFA0502800), the National Natural Science Foundation of China (31571083, 31970931), the Program for Professor of Special Appointment (Eastern Scholar of Shanghai, TP2014008), the Shanghai Municipal Science and Technology Major Project (No. 2017SHZDZX01) and ZJLab, the Shanghai Rising-Star Program (14QA1400800), E-Institutes of Shanghai Municipal Education Commission (E09013) and Shanghai Sailing Program (18YF1406600). We also thank the Supercomputer Center of East China Normal University (ECNU Multifunctional Platform for Innovation 001) for providing us computational time. The funders had no role in study design, data collection and analysis, decision to publish, or preparation of the manuscript.

Appendix A. Supplementary data

Supplementary data to this article can be found online at <https://doi.org/10.1016/j.heares.2020.107884>.

References

Abdelfatah, N., McComiskey, D.A., Doucette, L., Griffin, A., Moore, S.J., Negrijn, C., Hodgkinson, K.A., King, J.J., Larijani, M., Houston, J., Stanton, S.G., Young, T.L., 2013. Identification of a novel in-frame deletion in *KCNQ4* (*DFNA2A*) and evidence of multiple phenocopies of unknown origin in a family with ADSNHL. *Eur. J. Hum. Genet.* 21, 1112–1119.

Abraham, M.J., Murtola, T., Schulz, R., Páll, S., Smith, J.C., Hess, B., Lindahl, E., 2015. GROMACS: high performance molecular simulations through multi-level parallelism from laptops to supercomputers. *SoftwareX* 1, 19–25.

Akita, J., Abe, S., Shinkawa, H., Kimberling, W.J., Usami, S., 2001. Clinical and genetic features of nonsyndromic autosomal dominant sensorineural hearing loss: *KCNQ4* is a gene responsible in Japanese. *J. Hum. Genet.* 46, 355–361.

Arnett, J., Emery, S.B., Kim, T.B., Boerst, A.K., Lee, K., Leal, S.M., Lesperance, M.M., 2011. Autosomal dominant progressive sensorineural hearing loss due to a novel mutation in the *KCNQ4* gene. *Arch. Otolaryngol. Head Neck Surg.* 137, 54–59.

Baek, J.I., Park, H.J., Park, K., Choi, S.J., Lee, K.Y., Yi, J.H., Friedman, T.B., Drayna, D., Shin, K.S., Kim, U.K., 2011. Pathogenic effects of a novel mutation (c.664_681del) in *KCNQ4* channels associated with auditory pathology. *Biochim. Biophys. Acta* 1812, 536–543.

Barrese, V., Stott, J.B., Greenwood, I.A., 2018. *KCNQ*-encoded potassium channels as therapeutic targets. *Annu. Rev. Pharmacol. Toxicol.* 58, 625–648.

Bateman, A., Martin, M.J., O'Donovan, C., Magrane, M., Apweiler, R., Alpi, E., Antunes, R., Ar-Ganiska, J., Bely, B., Bingley, M., Bonilla, C., Britto, R., Bursteinas, B., Chavali, G., Cibrian-Uhalte, E., Da Silva, A., De Giorgi, M., Dogan, T., Fazzini, F., Gane, P., Cas-Tro, L.G., Garmiri, P., Hatton-Ellis, E., Hieta, R., Huntley, R., Legge, D., Liu, W.D., Luo, J., MacDougall, A., Mutowo, P., Nightingale, A., Orchard, S., Pichler, K., Poggioli, D., Pundir, S., Pureza, L., Qi, G.Y., Rosanoff, S., Saidi, R., Sawford, T., Shypitsyna, A., Turner, E., Volynkin, V., Wardell, T., Watkins, X., Watkins, C., Figueira, L., Li, W.Z., McWilliam, H., Lopez, R., Xenarios, I., Bougueleret, L., Bridge, A., Poux, S., Redaschi, N., Aimo, L., Argoud-Puy, G., Auchincloss, A., Axelsen, K., Bansal, P., Baratin, D., Blatter, M.C., Boeckmann, B., Bolleman, J., Boutet, E., Breuza, L., Casal-Casas, C., De Castro, E., Coudert, E., Cucho, B., Doche, M., Dornevil, D., Duvaud, S., Estreicher, A., Famiglietti, L., Feuermann, M., Gasteiger, E., Gehant, S., Gerritsen, V., Gos, A., Gruaz-Gumowski, N., Hinz, U., Hulo, C., Jungo, F., Keller, G., Lara, V., Lemerrier, P., Lieberherr, D., Lombardot, T., Martin, X., Masson, P., Morgat, A., Neto, T.,

Nouspikel, N., Paesano, S., Pedruzzi, I., Pilbout, S., Pozzato, M., Pruess, M., et al., 2015. UniProt: a hub for protein information. *Nucleic Acids Res.* 43, D204–D212.

Berendsen, H.J., Postma, J.v., van Gunsteren, W.F., DiNola, A., Haak, J., 1984. Molecular dynamics with coupling to an external bath. *J. Chem. Phys.* 81, 3684–3690.

Bientinesi, R., Mancuso, C., Martire, M., Bassi, P.F., Sacco, E., Curro, D., 2017. Kv7 channels in the human detrusor: channel modulator effects and gene and protein expression. *Naunyn-Schmiedeberg's Arch. Pharmacol.* 390, 127–137.

Bussi, G., Donadio, D., Parrinello, M., 2007. Canonical sampling through velocity rescaling. *J. Chem. Phys.* 126.

Chadha, P., Jepps, T., Carr, G., Stott, J., Zhu, H., 2014. Contribution of Kv7.4/Kv7.5 heteromers to intrinsic and calcitonin gene-related peptide-induced cerebral reactivity. *Arterioscler. Thromb. Vasc. Biol.* 34, 887–893.

Coucke, P.J., Van Hauwe, P., Kelley, P.M., Kunst, H., Schatteman, I., Van Velzen, D., Meyers, J., Ensink, R.J., Verstreken, M., Declau, F., Marres, H., Kastury, K., Bhasin, S., McGuirt, W.T., Smith, R.J., Cremers, C.W., Van de Heyning, P., Willems, P.J., Smith, S.D., Van Camp, G., 1999. Mutations in the *KCNQ4* gene are responsible for autosomal dominant deafness in four *DFNA2* families. *Hum. Mol. Genet.* 8, 1321–1328.

de Heer, A.M., Schraders, M., Oostrik, J., Hoefsloot, L., Huygen, P.L., Cremers, C.W., 2011. Audioprofile-directed successful mutation analysis in a *DFNA2/KCNQ4* (p.Leu274His) family. *Ann. Otol. Rhinol. Laryngol.* 120, 243–248.

Eswar, N., Eramian, D., Webb, B., Shen, M.Y., Sali, A., 2008. Protein structure modeling with MODELLER. *Methods Mol. Biol.* 426, 145–159.

Goldstein, J.A., Lalwani, A.K., 2002. Further evidence for a third deafness gene within the *DFNA2* locus. *Am. J. Med. Genet.* 108, 304–309.

Gunthorpe, M.J., Large, C.H., Sankar, R., 2012. The mechanism of action of retigabine (ezogabine), a first-in-class K⁺ channel opener for the treatment of epilepsy. *Epilepsia* 53, 412–424.

Hansen, H.H., Waroux, O., Seutin, V., Jentsch, T.J., Aznar, S., Mikkelsen, J.D., 2008. Kv7 channels: interaction with dopaminergic and serotonergic neurotransmission in the CNS. *J. Physiol.* 586, 1823–1832.

Hess, B., Bekker, H., Berendsen, H.J.C., Fraaije, J.G.E.M., 1997. LINC: a linear constraint solver for molecular simulations. *J. Comput. Chem.* 18, 1463–1472.

Hildebrand, M.S., Tack, D., McMordie, S.J., DeLuca, A., Hur, I.A., Nishimura, C., Huygen, P., Casavant, T.L., Smith, R.J.H., 2008. Audioprofile-directed screening identifies novel mutations in *KCNQ4* causing hearing loss at the *DFNA2* locus. *Genet. Med.* 10, 297–304.

Huang, B., Liu, Y., Gao, X., Xu, J., Dai, P., Zhu, Q., Yuan, Y., 2017. A novel pore-region mutation, c.887G > A (p.G296D) in *KCNQ4*, causing hearing loss in a Chinese family with autosomal dominant non-syndromic deafness 2. *BMC Med. Genet.* 18, 36.

Iannotti, F.A., Barrese, V., Formisano, L., Miceli, F., Tagliatela, M., 2013. Specification of skeletal muscle differentiation by repressor element-1 silencing transcription factor (REST)-regulated Kv7.4 potassium channels. *Mol. Biol. Cell* 24, 274–284.

Ishikawa, K., Naito, T., Nishio, S.Y., Iwasa, Y., Nakamura, K., Usami, S., Ichimura, K., 2014. A Japanese family showing high-frequency hearing loss with *KCNQ4* and *TECTA* mutations. *Acta Otolaryngol.* 134, 557–563.

Jepps, T.A., Greenwood, I.A., Moffatt, J.D., Sanders, K.M., Ohya, S., 2009. Molecular and functional characterization of Kv7 K⁺ channel in murine gastrointestinal smooth muscles. *Am. J. Physiol. Gastrointest. Liver Physiol.* 297, G107–G115.

Jepps, T.A., Chadha, P.S., Davis, A.J., Harhun, M.I., Cockerill, G.W., Olesen, S.P., Hansen, R.S., Greenwood, I.A., 2011. Downregulation of Kv7.4 channel activity in primary and secondary hypertension. *Circulation* 124, 602–611.

Jung, J., Choi, H.B., Koh, Y.I., Rim, J.H., Choi, H.J., Kim, S.H., Lee, J.H., An, J., Kim, A., Lee, J.S., Joo, S.Y., Yu, S., Choi, J.Y., Kang, T.M., Gee, H.Y., 2018. Whole-exome sequencing identifies two novel mutations in *KCNQ4* in individuals with non-syndromic hearing loss. *Sci. Rep.* 8, 16659.

Kamada, F., Kure, S., Kudo, T., Suzuki, Y., Oshima, T., Ichinohe, A., Kojima, K., Niihori, T., Kanno, J., Narumi, Y., Narisawa, A., Kato, K., Aoki, Y., Ikeda, K., Kobayashi, T., Matsubara, Y., 2006. A novel *KCNQ4* one-base deletion in a large pedigree with hearing loss: implication for the genotype-phenotype correlation. *J. Hum. Genet.* 51, 455–460.

Kharkovets, T., Hardelin, J.P., Safieddine, S., Schweizer, M., El-Amraoui, A., Petit, C., Jentsch, T.J., 2000. *KCNQ4*, a K⁺ channel mutated in a form of dominant deafness, is expressed in the inner ear and the central auditory pathway. *Proc. Natl. Acad. Sci. U.S.A.* 97, 4333–4338.

Kharkovets, T., Dedek, K., Maier, H., Schweizer, M., Khimich, D., Nouvian, R., Vardanyan, V., Leuwer, R., Moser, T., Jentsch, T.J., 2006. Mice with altered *KCNQ4* K⁺ channels implicate sensory outer hair cells in human progressive deafness. *EMBO J.* 25, 642–652.

Kholmurodov, K., Smith, W., Yasuoka, K., Darden, T., Ebisuzaki, T., 2000. A smooth-particle mesh Ewald method for DL-POLY molecular dynamics simulation package on the Fujitsu VPP700. *J. Comput. Chem.* 21, 1187–1191.

Kim, H.J., Lv, P., Sihh, C.R., Yamoah, E.N., 2011. Cellular and molecular mechanisms of autosomal dominant form of progressive hearing loss, *DFNA2*. *J. Biol. Chem.* 286, 1517–1527.

Klauda, J.B., Venable, R.M., Freites, J.A., O'Connor, J.W., Tobias, D.J., Mondragon-Ramirez, C., Vorobyov, I., MacKerell, A.D., Pastor, R.W., 2010. Update of the CHARMM all-atom additive force field for lipids: validation on six lipid types. *J. Phys. Chem. B* 114, 7830–7843.

Kubisch, C., Schroeder, B.C., Friedrich, T., Lutjohann, B., El-Amraoui, A., Marlin, S., Petit, C., Jentsch, T.J., 1999. *KCNQ4*, a novel potassium channel expressed in sensory outer hair cells, is mutated in dominant deafness. *Cell* 96, 437–446.

Leitner, M.G., Feuer, A., Ebers, O., Schreiber, D.N., Halaszovich, C.R., Oliver, D., 2012. Restoration of ion channel function in deafness-causing *KCNQ4* mutants by

- synthetic channel openers. *Br. J. Pharmacol.* 165, 2244–2259.
- Long, S.B., Campbell, E.B., MacKinnon, R., 2005. Crystal structure of a mammalian voltage-dependent Shaker family K⁺ channel. *Science* 309, 897–903.
- Mencia, A., Gonzalez-Nieto, D., Modamio-Hoybjor, S., Etxeberria, A., Aranguiz, G., Salvador, N., Del Castillo, I., Villarroel, A., Moreno, F., Barrio, L., Moreno-Pelayo, M.A., 2008. A novel *KCNQ4* pore-region mutation (p.G296S) causes deafness by impairing cell-surface channel expression. *Hum. Genet.* 123, 41–53.
- Naito, T., Nishio, S.Y., Iwasa, Y., Yano, T., Kumakawa, K., Abe, S., Ishikawa, K., Kojima, H., Namba, A., Oshikawa, C., Usami, S., 2013. Comprehensive genetic screening of *KCNQ4* in a large autosomal dominant nonsyndromic hearing loss cohort: genotype-phenotype correlations and a founder mutation. *PLoS One* 8, e63231.
- Namba, K., Mutai, H., Kaneko, H., Hashimoto, S., Matsunaga, T., 2012. *In silico* modeling of the pore region of a *KCNQ4* missense mutant from a patient with hearing loss. *BMC Res. Notes* 5, 145.
- Posukh, O., Pallares-Ruiz, N., Tadinova, V., Osipova, L., Claustres, M., Roux, A.F., 2005. First molecular screening of deafness in the Altai Republic population. *BMC Med. Genet.* 6, 12.
- Rudzinski, L.A., Velez-Ruiz, N.J., Gedzelman, E.R., Mauricio, E.A., Shih, J.J., Karakis, I., 2016. New antiepileptic drugs: focus on ezogabine, clobazam, and perampanel. *J. Investig. Med.* 64, 1087–1101.
- Sheppard, A.M., Chen, G.D., Salvi, R., 2015. Potassium ion channel openers, Maxipost and Retigabine, protect against peripheral salicylate ototoxicity in rats. *Hear. Res.* 327, 1–8.
- Shin, D.H., Jung, J., Koh, Y.I., Rim, J.H., Lee, J.S., Choi, H.J., Joo, S.Y., Yu, S., Cha, D.H., Lee, S.Y., Lee, J.H., Lee, M.G., Choi, J.Y., Gee, H.Y., 2018. A recurrent mutation in *KCNQ4* in Korean families with nonsyndromic hearing loss and rescue of the channel activity by KCNQ activators. *Hum. Mutat.*
- Su, C.C., Yang, J.J., Shieh, J.C., Su, M.C., Li, S.Y., 2007. Identification of novel mutations in the *KCNQ4* gene of patients with nonsyndromic deafness from Taiwan. *Audiol. Neurotol.* 12, 20–26.
- Sun, J., MacKinnon, R., 2017. Cryo-EM structure of a *KCNQ1*/CaM complex reveals insights into congenital long QT syndrome. *Cell* 169, 1042–+.
- Talebizadeh, Z., Kelley, P.M., Askew, J.W., Beisel, K.W., Smith, S.D., 1999. Novel mutation in the *KCNQ4* gene in a large kindred with dominant progressive hearing loss. *Hum. Mutat.* 14, 493–501.
- Testai, L., Barrese, V., Soldovieri, M.V., Ambrosino, P., Martelli, A., Vinciguerra, I., Miceli, F., Greenwood, I.A., Curtis, M.J., Breschi, M.C., Sisalli, M.J., Scorziello, A., Canduela, M.J., Grandes, P., Calderone, V., Tagliatalata, M., 2016. Expression and function of Kv7.4 channels in rat cardiac mitochondria: possible targets for cardioprotection. *Cardiovasc. Res.* 110, 40–50.
- Topsakal, V., Pennings, R.J., te Brinke, H., Hamel, B., Huygen, P.L., Kremer, H., Cremers, C.W., 2005. Phenotype determination guides swift genotyping of a DFNA2/*KCNQ4* family with a hot spot mutation (W276S). *Otol. Neurotol.* 26, 52–58.
- Uehara, D.T., Freitas, E.L., Alves, L.U., Mazzeu, J.F., Auricchio, M.T., Tabith Jr., A., Monteiro, M.L., Rosenberg, C., Mingroni-Netto, R.C., 2015. A novel *KCNQ4* mutation and a private *IMMP2L-DOCK4* duplication segregating with nonsyndromic hearing loss in a Brazilian family. *Hum. Genome Var.* 2, 15038.
- Van Camp, G., Coucke, P.J., Akita, J., Fransen, E., Abe, S., De Leenheer, E.M., Huygen, P.L., Cremers, C.W., Usami, S., 2002. A mutational hot spot in the *KCNQ4* gene responsible for autosomal dominant hearing impairment. *Hum. Mutat.* 20, 15–19.
- Van Hauwe, P., Coucke, P.J., Ensink, R.J., Huygen, P., Cremers, C.W., Van Camp, G., 2000. Mutations in the *KCNQ4* K⁺ channel gene, responsible for autosomal dominant hearing loss, cluster in the channel pore region. *Am. J. Med. Genet.* 93, 184–187.
- Wang, H., Zhao, Y., Yi, Y., Gao, Y., Liu, Q., Wang, D., Li, Q., Lan, L., Li, N., Guan, J., Yin, Z., Han, B., Zhao, F., Zong, L., Xiong, W., Yu, L., Song, L., Yi, X., Yang, L., Petit, C., Wang, Q., 2014. Targeted high-throughput sequencing identifies pathogenic mutations in *KCNQ4* in two large Chinese families with autosomal dominant hearing loss. *PLoS One* 9, e103133.
- Wang, J.J., Li, Y., 2016. KCNQ potassium channels in sensory system and neural circuits. *Acta Pharmacol. Sin.* 37, 25–33.
- Wang, L., Qiao, G.H., Hu, H.N., Gao, Z.B., Nan, F.J., 2019. Discovery of novel retigabine derivatives as potent *KCNQ4* and *KCNQ5* channel agonists with improved specificity. *ACS Med. Chem. Lett.* 10, 27–33.
- Wasano, K., Mutai, H., Obuchi, C., Masuda, S., Matsunaga, T., 2015. A novel frameshift mutation in *KCNQ4* in a family with autosomal recessive non-syndromic hearing loss. *Biochem. Biophys. Res. Commun.* 463, 582–586.
- Watabe, T., Matsunaga, T., Namba, K., Mutai, H., Inoue, Y., Ogawa, K., 2013. Moderate hearing loss associated with a novel *KCNQ4* non-truncating mutation located near the N-terminus of the pore helix. *Biochem. Biophys. Res. Commun.* 432, 475–479.
- Wei, X., Zhang, Y., Yin, B., Wen, J., Cheng, J., Fu, X., 2018. The expression and function of KCNQ potassium channels in human chorionic plate arteries from women with normal pregnancies and pre-eclampsia. *PLoS One* 13, e0192122.
- Wu, C.C., Lin, Y.H., Lu, Y.C., Chen, P.J., Yang, W.S., Hsu, C.J., Chen, P.L., 2013. Application of massively parallel sequencing to genetic diagnosis in multiplex families with idiopathic sensorineural hearing impairment. *PLoS One* 8, e57369.